Article

Assessing the Relationship between Land Surface Temperature and Composition Elements of Urban Green Spaces during Heat Waves Episodes in Mediterranean Cities

Manuel José Delgado-Capel [1], **Paloma Egea-Cariñanos** [2] **and Paloma Cariñanos** [1,3,*]

1 Department of Botany, University of Granada, Cartuja Campus, 18071 Granada, Spain; mdelgado@correo.ugr.es
2 Department of Political Science, University of Granada, Fuentenueva Campus, 18071 Granada, Spain; palomaegeac@ugr.es
3 Andalusian Institute for Earth System Research (IISTA-CEAMA), University of Granada, 18100 Granada, Spain
* Correspondence: palomacg@ugr.es

Abstract: In the context of escalating global temperatures and intensified heat waves, the Mediterranean region emerges as a noteworthy hotspot, experiencing a surge in the frequency and intensity of these extreme heat events. Nature-based solutions, particularly management of urban green infrastructure (UGI) areas, have shown promising outcomes in adapting urban areas to the challenges posed by heat waves. The objective of the current study is twofold: firstly, to identify the compositional patterns of strategically distributed small public green spaces, demonstrating their enhanced capacity to mitigate the impact of heat waves in the Mediterranean region; secondly, to assess the association, direction, and explanatory strength of the relationship between the composition elements of the UGI areas and area typology, specifically focusing on the variation in land surface temperature (LST) values during heat wave episodes spanning from 2017 to 2023. The methodology involved obtaining land surface temperature (LST) values from satellite images and classifying green areas based on composition, orientation, and typology. Ordinal multiple regressions were conducted to analyze the relationship between the considered variables and LST ranges during heat wave episodes that occurred from 2017 to 2023. The findings indicate an increase in LST ranges across many areas, emphasizing heightened thermal stress in a Mediterranean medium-sized compact city, Granada (in the southeast of the Iberian Peninsula). Traditional squares, pocket parks and gardens, and pedestrian areas with trees and impervious surfaces performed better in reducing the probability of exceeding LST values above 41 °C compared to other vegetated patches mainly occupied by herbaceous vegetation and grass. The study concludes by advocating for the strategic incorporation of vegetation, especially trees, along with traditional squares featuring semipermeable pavement with trees and shrubbery, as a potential effective strategy for enhancing resilience against extreme heat events. Overall, this research enhances our understanding of LST dynamics during heat waves and offers guidance for bolstering the resilience of urban green spaces in the Mediterranean region.

Keywords: climate change adaptation; small public urban green spaces; compact city; urban green infrastructure; heat waves; urban cooling capacity; green spaces composition; Mediterranean traditional squares; UGI design; green areas composition

1. Introduction

Escalating global temperatures and the heightened frequency and intensity of heat waves (HWs) have become prominent focal points in climate change research, with significant implications for health, energy, and ecological aspects [1–3]. Officially confirmed by international datasets as the warmest year on record, 2023 underscores the urgency of addressing these climatic shifts [4,5]. The latest Intergovernmental Panel on Climate Change

(IPCC) Sixth Assessment Report highlights the robust evidence of increased warm days and extreme temperatures globally, with a particular emphasis on HWs in the southern Mediterranean [6].

In this context, the Mediterranean region stands out as a heat hotspot, experiencing a rising trend in the average intensity and frequency of HWs, along with an increase in minimum temperatures [7–9]. In particular, this forecast has direct effects, especially in urban areas, which, among other impacts, result in heat stress and related issues detrimental to human well-being [10–12]. Notably, higher surface temperature values are associated with increased risk of mortality and morbidity during heat waves [13–15]. In this context, green areas can play a crucial role in outdoor environments, effectively mitigating high temperatures and providing a protective shield against heat-related impacts [16]. The significance of green spaces becomes particularly evident in Mediterranean climate cities, as revealed by a health impact assessment conducted by Iungman et al. (2023). That study showed how cities with low cooling index scores, such as Athens, Valencia, Seville, Palermo, Málaga, and Madrid, experienced elevated mortality rates due to heat stress. Specifically, the effect of summer on annual attributable deaths (95% CI) ranged from 12.39% in Málaga to 14.82% in Barcelona. Moreover, an increase in tree coverage demonstrated its potential to generate a notable decrease in summer preventable deaths, as seen in Murcia with a reduction of 29.85% (95% CI) [17]. Additionally, previous research in the Mediterranean region emphasizes effective and very specific strategies at different scales to face these challenges. At the microscale level, establishing and promoting habitable spaces, such as courtyards, and implementing shading strategies have demonstrated positive outcomes during HW episodes [18,19]. Increasing green spaces with vegetation at a local level has also been demonstrated as a successful measure [20]. Ultimately, applicable across all scales within urban areas and serving as more comprehensive strategies to adapt and mitigate the impacts of HWs, are nature-based solutions [21,22]. As a nature-based solution, management of urban green infrastructure (UGI) areas provides highly effective outcomes in adapting urban areas to the anticipated challenges posed by future HWs [23]. While increasing vegetation and greening strategies in UGI areas represent a well-fitted adaptation and mitigation strategy, additional research becomes crucial to determine the most suitable UGI for specific urban areas to strengthen the buffer capacity against the impacts of warm spells [24,25].

In a recent study conducted by Delgado et al. in 2023, an in-depth investigation into the cooling capacity of green spaces during HW episodes was undertaken [26]. This involved a meticulous examination of the correlation between land surface temperature (LST) and the Normalized Difference Vegetation Index. Despite some existing pitfalls in the literature that suggest a potential link between "warm surfaces" and "high air temperatures", particularly in urban heat-island-related studies, LST is considered a reliable proxy for air temperature and thermal comfort [27–30]. In addition to the quantity, health, and type of vegetation, LST values respond to urban land surface properties by detecting variations in spectral reflectance between built-up or impervious surfaces and the brightness of surface or bare soil cover [31]. Building upon this understanding, the premise of the current study is grounded. It posits that small green spaces strategically distributed across urban areas could play a pivotal role in mitigating the impacts of HW episodes, especially in medium-sized compact cities within the Mediterranean region. In Delgado et al. (2023) [26], these smaller green spaces exhibited greater cooling capacity against extreme temperatures during HWs compared to medium-sized patches (with extensions ranging from 10,000 m^2 to 100,000 m^2), including small forests, dense shrubs, grasslands, or parks. Additionally, they showed better cooling capacity compared to areas with linear spatial distributions that connect larger-sized patches (with extensions exceeding 100,000 m^2), such as urban forests, to medium-sized ones. While it is commonly acknowledged that larger urban parks exhibit a higher cooling effect intensity, as indicated by the temperature difference compared to vegetation-free urban areas [32], smaller urban green spaces stand out for their capability to extend cooling effects over a greater distance than some larger

areas, which enhances benefits at the microsite level, such as within neighborhoods or residential clusters [33,34]. These smaller green spaces have the potential to significantly and effectively reduce the LST in their surroundings, contributing to the improvement in the urban thermal environment, particularly in high-density urban settings [35]. With this backdrop, optimizing the cooling effects of these small urban green spaces requires a detailed understanding of their types and composition elements [36]. However, the design and composition elements of these UGI assets poses challenges, encompassing factors such as adaptability to extreme [37], sudden, and fluctuating weather conditions, and considerations of the physical footprint [38,39], potential ecosystem disservices [40], accessibility [41], or the influence of size and design on perceived well-being [42].

In this context, the primary objective of the current study is twofold. Firstly, it aims to identify the compositional patterns of small public green spaces scattered heterogeneously throughout the urban matrix, showcasing enhanced capacity to ameliorate the impact of HWs in the Mediterranean region, as indicated by previous research [26]. Secondly, this study aims to evaluate the association, direction, and explanatory strength in the relationship between the composition elements of the UGI areas under study and the area typology, concerning the variation of LST values during HW episodes spanning from 2017 to 2023. Finally, the research strives to elucidate which components of these smaller green areas and what typology of green space enhance the buffer capacity against the impacts of warm spells, thereby providing valuable insights into the ongoing discourse on urban heat mitigation strategies.

2. Materials and Methods

2.1. Study Area

Granada is a representative medium-sized compact city of the Mediterranean region located in the southeast of the Iberian Peninsula (37.179937, −3.603489; 680 m. a.s.l.). In the urban area of Granada, an excessive coverage of built-up areas can be observed, with a 12.42% increase between 2002 and 2022 [20]. The average percentage of the built-up area in 2022 varied from 39.37% in areas characterized by high-density urban fabric to 87.28% in the dense urban core [43]. It presents a Mediterranean–continental climate, with an average annual temperature of 15.2 °C for the period of 1985–2014 (which is projected to increase to 16.8 °C by 2050) [44]. The Köppen–Geiger climate classification for Granada is Csa, which corresponds to a Mediterranean climate characterized by dry and hot summers [45,46]. Since 1975, Granada has been significantly impacted by heat waves, exhibiting the highest recurrence rate of these events since 2011 among Spanish cities [47].

Of the 341 areas within Granada's urban green infrastructure (UGI), this study specifically concentrated on the analysis of smaller public urban green spaces classified as "Other" areas [48]. It is important to note that a portion of these areas (14.07%) exceeds the characteristic size limit set for a small public urban green space (SPUGS), which is defined as an area below 5000 m^2 [49] (Figure 1).

2.2. Heat Wave Identification and Land Surface Temerature Retrieval

This research adopted the heat wave (HW) definition given by the Spanish Agency of Meteorology (AEMET) as an episode lasting at least three consecutive days, during which at least 10% of the considered weather stations record maximum temperatures above the 95th percentile of their daily maximum temperature series for the months of July and August during the 1971–2000 period [50].

Land surface temperature (LST) values in daylight hours for each target area were obtained from a previous study by Delgado-Capel et al. (2023) [26] using Landsat 8 and 9 OLI/TIRS satellite images derived from the U.S. Geological Survey [51]. To address the stated objectives, in this study, we selected maximum LST values based on the consideration of the cumulative adverse impacts of higher temperatures during extreme heat episodes [52,53]. The LST datasets were updated with the latest data corresponding to the HWs identified in 2023 [54]. A total of 16 episodes were identified, among which

LST retrieval was only possible in 11 of them. This limitation arose due to the absence of Landsat images on required dates or cloud coverage obstructing the proper LST retrieval over the target areas within the urban matrix (Table 1).
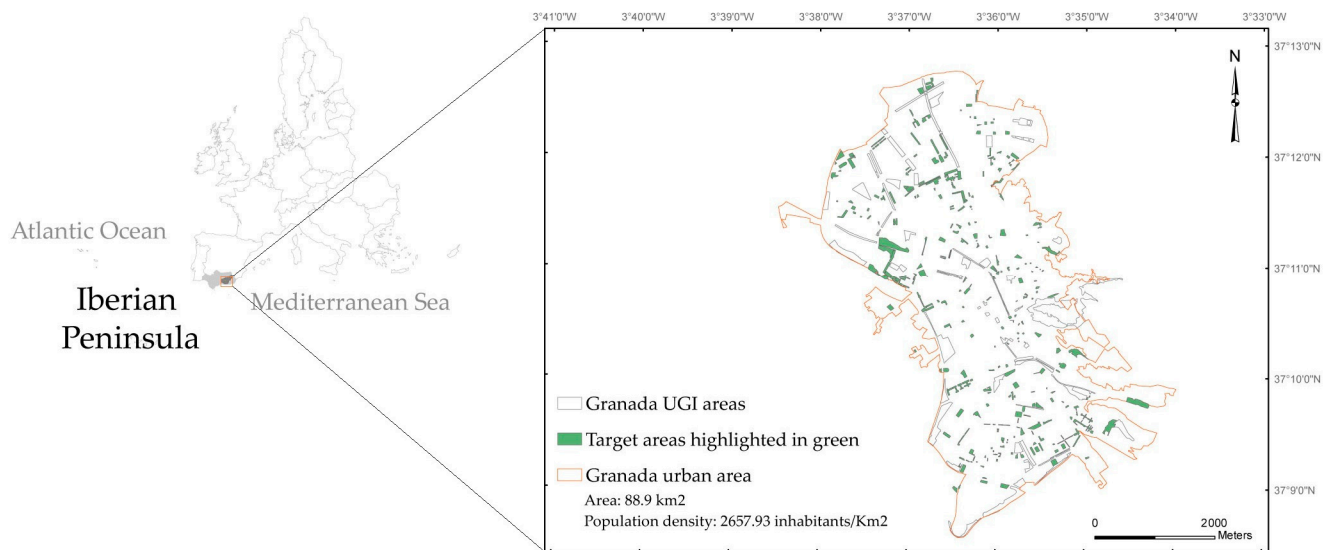

Figure 1. Smaller urban green spaces within the urban green infrastructure of the study area.

Table 1. Heat wave episode information and Landsat image details.

HW [1] Episode	Start–End Dates	Duration	Data Source [2]	Date Acquired	Scene Center Time (GMT + 1) [3]
HW 1	13–21 June 2017	9 days	Landsat 8 (OLI/TIRS)	19 June 2017	11:49:55
HW 2	12–16 July 2017	5 days	Landsat 8 (OLI/TIRS)	Not available on required dates	
HW 3	28–30 July 2017	3 days	Landsat 8 (OLI/TIRS)	Not available on required dates	
HW 4	2–6 August 2017	5 days	Landsat 8 (OLI/TIRS)	Cloud cover above the urban matrix	
HW 5	31 July–7 August 2018	8 days	Landsat 8 (OLI/TIRS)	9 August 2018	11:49:50
HW 6	26 June–1 July 2019	6 days	Landsat 8 (OLI/TIRS)	25 June 2019	11:50:04
HW 7	20–25 July 2019	6 days	Landsat 8 (OLI/TIRS)	18 July 2019	11:56:19
HW 8	25 July–2 August 2020	9 days	Landsat 8 (OLI/TIRS)	29 July 2020	11:50:08
HW 9	6–8 August 2020	5 days	Landsat 8 (OLI/TIRS)	5 August 2020	11:56:20
HW 10	11–16 August 2021	6 days	Landsat 8 (OLI/TIRS)	17 August 2021	11:50:21
HW 11	12–18 June 2022	7 days	Landsat 9 (OLI/TIRS)	9 June 2022	11:49:43
HW 12	9–26 July 2022	18 days	Landsat 8 (OLI/TIRS)	19 July 2022	11:50:28
HW 13	9–12 July 2023	4 days	Landsat 8 (OLI/TIRS)	Not available on required dates	
HW 14	17–20 July 2023	4 days	Landsat 8 (OLI/TIRS)	Cloud cover above the urban matrix	
HW 15	6–13 August 2023	8 days	Landsat 8 (OLI/TIRS)	7 August 2023	11:50:03
HW 16	17–25 August 2023	9 days	Landsat 8 (OLI/TIRS)	23 August 2023	11:50:11

[1]: HW#: Heat wave episode; [2]: OLI/TIRS: Operational Land Imager Thermal Infrared Sensor; [3]: GMT: Global Meridian Time.

Land surface temperature (LST) values were recoded into specific ranges to facilitate a comprehensive understanding of their distribution and their association with areas prone to discomfort due to heat stress. To carry out this recoding, this study supported the approach on the significant correlation between LST, air temperature, and the Physiological Equivalent Temperature (PET) [55,56]. PET is among the most widely employed thermal indices in urban settings, renowned for its ability to intricately consider complex urban geometries and surfaces and its applicability in studies assessing the impact and perception of heat waves in cities [57,58]. The adopted recoding of LST values was aligned with the indicative PET thresholds for regions similar to our study area, in which temperatures below 35 °C trigger a moderate heat stress (warm thermal sensation), while temperatures exceeding 41 °C trigger extreme heat stress (very hot thermal sensation) [59–61]. Prior research conducted in the Mediterranean region employed intervals of 2 degrees for setting up the ranges [62,63]. Therefore, LST values were eventually recoded into 5 ranges, as shown in Table 2.

Table 2. Summary of variable recoding: ranges of land surface temperature values, intervals of cover percentage for composition elements, and orientation assigned to the target areas based on their major axis.

Land Surface Temperature (LST)		Percentage Coverage of Composition Elements			Orientation	
LST Interval (°C)	LST Range	Variables		Intervals of Cover Percentage	Major Axis Orientation	Assignation [6]
<35.00	LST Range 1	Tree	Imp. Surf. [4]	1: 0–20.00		
35.01–37.00	LST Range 2	Shrub	Build	2: 20.01–40.00	45.01° to 135.00°	
37.01–39.00	LST Range 3	Herb/Grass [1]	C/G/P [5]	3: 40.01–60.00	225.01° to 315.00°	EW
39.01–41.00	LST Range 4	Soil [2]	Water	4: 60.01–80.00	315.01° to 45.00°	
>41.01	LST Range 5	Perv. Surf. [3]		5: 80.01–100%	135.01° to 225.00°	NS

[1]: Herb/Grass: herbaceous species and grasses; [2]: Soil: bare soil; [3]: Perv. Surf.: pervious surfaces; [4]: Imp. Surf.: impervious surfaces; [5]: C/G/P: cobblestone, gravel, and pebble; [6]: EW: East–West, NS: North–South.

2.3. Composition and Orientation of Target Areas

The composition of elements within the target areas, included trees, shrubs, surfaces with herbaceous species and grasses, bare soil, pervious surfaces (such as sands or silts), impervious surfaces (such as asphalt, concrete, construction tiles or rubberized surfaces), buildings, and water surfaces (mainly found in square fountains). In addition, semipermeable pavement was included as a structural component, as it is a type of surface widely found in parks and squares of compact medium- and small-sized cities in the Mediterranean region due to its historical heritage [64]. This type of surface mainly combines rounded pebbles, cobblestones, or gravel with permeable interstitial spaces.

The identification of composition elements was performed by calculating the percentage coverage for each composition element in every target area with ARCGIS 10.6 software. This process involved visualizing and identifying each composition element within each target area using high-resolution aerial orthophotography coverage from the National Aerial Orthophotography Plan [65]. This exhaustive and manual identification allowed us to overcome the existing challenges in land cover mapping and processing at this resolution [66], including accuracy limitations in distinguishing certain categories (e.g., dry grass or bare soil vs. concrete, trees vs. irrigated grass, or roofs vs. asphalt) [67] and potential issues with supervised learning techniques not providing fully ground-truth labels [68,69]. Subsequently, each target area was assigned a range of coverage percentage for each composition element, to enhance data simplicity and control over variability, and

to improve overall manageability and interpretability of results. The percentage coverage of elements was recoded into 5 ranges: 1 = 0%–20%, 2 = 20.01%–40%, 3 = 40.01%–60%, 4 = 60.01%–80%, and 5 = 80.01%–100% (Table 2).

Finally, the orientation of the target areas was determined based on the position of the major axis of each area. Thus, areas with their major axis oriented between 45 and 135 degrees, and from 225 to 315 degrees, were assigned an East–West orientation. Conversely, areas with their major axis oriented from 315 to 45 degrees, and from 135 to 225 degrees, were assigned a North–South orientation (Table 2).

2.4. Statistical Analysis

Ordinal regressions were computed for analyzing the effect of SPUGS components, orientation, and type (as independent variables) on LST ranges (as dependent variables). To test the association, direction, and strength of each composition and orientation variables in the explanatory power of the LST range reached in each event, 12 multiple ordinal regressions were modeled, one for each HW episode with available data and another one with the mean value of all episodes.

In each case, the dependent variable was the LST value collected in each HW episode recoded in segments and the independent variables were the recoded percentages of cover composition element and orientation. To test the levels of explanatory power of each model with respect to the null model, the Cox and Snell, and Nagelkerke and McFadden pseudo R-squared were used [70,71].

Subsequently, the composition element variables were grouped into type of SPUGS using the K-means clustering technique. To determine the number of clusters to extract, the elbow method was used, observing the loss of internal heterogeneity as the number of retained clusters increases. Where the slope decreases steeply, it is determined as the number of clusters to be obtained. Subsequently, the means of the variables in each cluster were analyzed, as well as the relationship of the clusters with the rest of the variables using chi-square and Haberman's corrected standardized residuals analysis, in order to name and interpret the type of SPUG under assessment.

Finally, with the intention of providing aggregate information on what type of SPUG reduces or increases to a greater extent the probability of reaching higher LST ranges, 12 new multiple ordinal regressions were performed in which the independent variables were each cluster, and each of the dependent variables comprised the LST values recoded in segments. The statistical analysis for this research was conducted using IBM SPSS Statistics software, version 28.0.0.0 (190).

3. Results

3.1. Land Surface Temperature Assessment

Data on land surface temperature (LST) were collected for 11 episodes spanning from 2017 to 2023, along with the overall mean for all episodes. The least intense HW episode was the latest recorded in 2019 (HW7), with a mean LST value of 32.53 °C across all areas. The highest mean LST value occurred in the first episode of 2020 (HW8), reaching 41.10 °C. Following this episode, LST mean values surpassed those of the initial episodes from 2017 and 2018 (HW1, HW5, and HW6), ranging from 39.12 °C in episode HW12 to 39.85 °C in the last episode recorded in 2023 (HW16). The overall mean LST across all episodes was 37.94 °C (Figure 2).
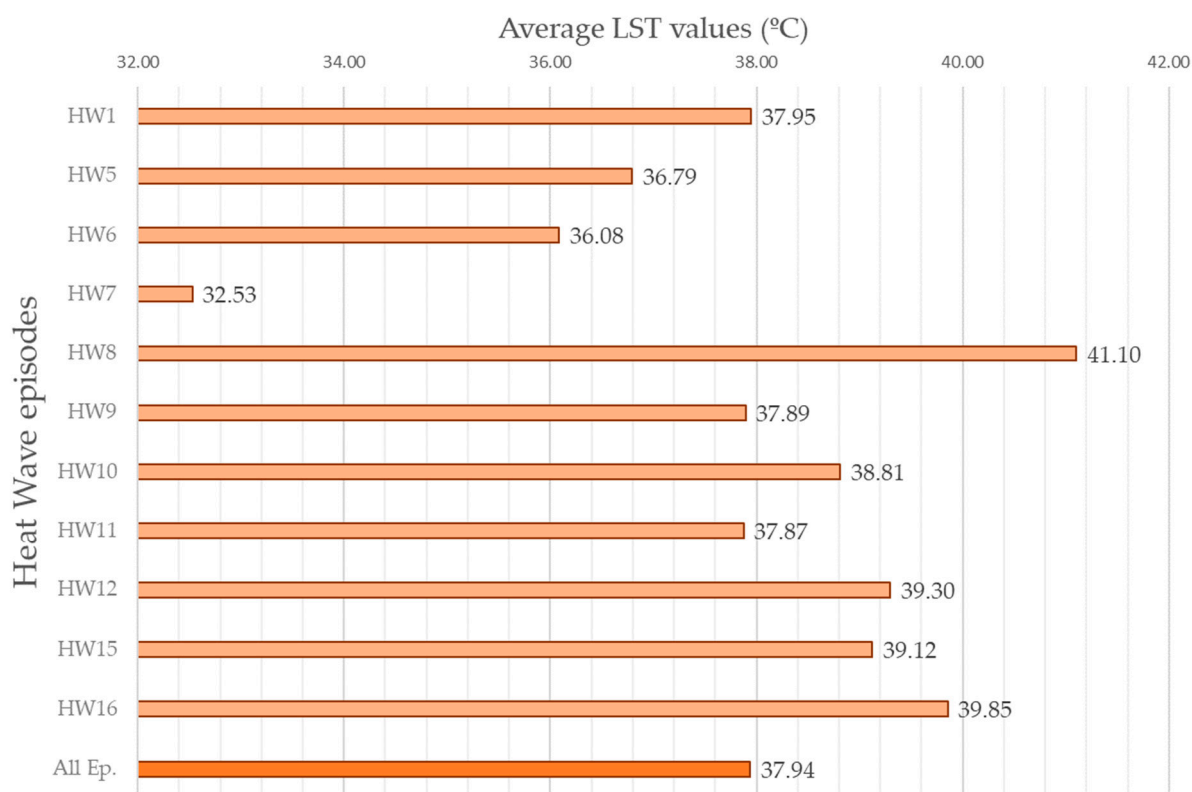
Figure 2. Average of retrieved LST values per heat wave (HW) episode and all episodes over the target areas.

The distribution of LST values within the adopted recoding ranges illustrates that LST Range 3 (values between 37.01–39.00 °C) and LST Range 4 (values between 39.01–41.00 °C) accumulated the highest percentage of areas falling within these ranges. In alignment with the average LST values per episode, 96.19% of the studied areas exhibited values below 35 °C in the latest HW episode recorded in 2019 (HW7). Conversely, in the hottest episode (HW8), 95.01% of the areas registered LST values above 39.01 °C, with 43.40% falling within LST Range 4 (values between 39.01–41.00 °C) and 56.61% within LST Range 5 (values above 41 °C). Considering all episodes, most of the studied areas (65.40%) recorded values between 37.01 and 39.00 °C (LST Range 3) (Table 3).

Table 3. Percentage of areas within the adopted land surface temperature (LST) ranges.

	LST Range 1	LST Range 2	LST Range 3	LST Range 4	LST Range 5
HW1	1.76%	17.89%	65.10%	10.85%	4.40%
HW5	6.16%	53.37%	35.48%	2.93%	2.05%
HW6	17.89%	64.22%	13.78%	2.93%	1.17%
HW7	96.19%	2.64%	0.59%	0.59%	0.00%
HW8	0.00%	1.17%	3.81%	43.40%	51.61%
HW9	2.64%	24.63%	57.77%	10.56%	4.40%
HW10	0.59%	3.81%	56.89%	32.84%	5.87%
HW11	0.88%	23.46%	62.46%	9.38%	3.81%
HW12	0.29%	2.05%	37.54%	52.79%	7.33%
HW15	0.29%	3.52%	46.04%	42.82%	7.33%
HW16	0.29%	2.05%	24.63%	54.84%	18.18%
All Ep.	0.88%	20.23%	65.40%	11.44%	2.05%

LST Range 1: <35.00 °C; LST Range 2: 35.01–37.00 °C; LST Range 3: 37.01–39.00 °C; LST Range 4: 39.01–41.00 °C; LST Range 5: >41.01 °C.

3.2. Information on Composition Elements and Clustering Result

In the identification of composition elements within the target areas, the most prevalent element was the impervious surface, with an average coverage percentage of 39.24% across all areas. Over 50% of areas with impervious surface presence exhibited less than 40.00% coverage. Trees showed a mean coverage of 27.25%, with 42.52% of areas having up to 20.00% tree coverage and 35.48% with coverage between 20.01% and 40%. The rest of the vegetated composition elements, shrub and herbaceous species/grasses, had average coverages of 7.47% and 9.78%, respectively, with 87.89% and 81.52% of areas having up to 20% coverage for shrubs and herbaceous species/grasses. Pervious surface had a mean coverage of 9.32%, with 79.77% of areas having up to 20% coverage. Semi-impermeable surfaces (cobblestone, gravel, pebble) averaged 4.34% and their presence in all areas was under 20.00% coverage. Bare soil had a mean coverage of 2.12%, present in 97.65% of areas with less than 20% coverage. Buildings showed a limited presence (0.44% average coverage), and water had a negligible presence (0.06% average coverage) in 100% of areas, with water presence not exceeding 3% of the total green area in any case (Table 4).

Table 4. Composition element assessment.

| Composition Element [1]	Tree	Shrub	Herb./Grass	Soil	Perv. Surface	Imp. Surface	Build	C/G/P	Water
Avg. All [2]	27.25%	7.47%	9.78%	2.12%	9.32%	39.24%	0.44%	4.34%	0.06%
Intervals of cover%				% of areas within each interval					
1: 0–20.00	42.52%	87.98%	81.52%	97.65%	79.77%	35.78%	99.41%	100.00%	100.00% [3]
2: 20.01–40.00	35.48%	9.09%	9.97%	0.59%	12.90%	15.25%	0.59%	0.00%	0.00%
3: 40.01–60.00	13.49%	2.64%	2.93%	0.59%	3.81%	19.65%	0.00%	0.00%	0.00%
4: 60.01–80.00	3.81%	0.29%	1.76%	0.59%	2.93%	17.30%	0.00%	0.00%	0.00%
5: 80.01–100%	4.69%	0.00%	3.52%	0.59%	0.59%	11.73%	0.00%	0.00%	0.00%

[1]: Composition elements: Herb/Grass: herbaceous species and grasses; Soil: soil and bare ground; Perv. Surf.: pervious surfaces; Imp. Surf.: impervious surfaces; C/G/P: cobblestone, gravel, and pebble; [2]: Cover average of each composition element in all areas. [3]: Presence of water in only 16 areas, under 3% of the total area surface and less than 100 m^2 in all cases.

The clustering of target areas resulted in four distinct types defined by their composition elements (Figure 3, Table 5):

- Traditional squares and parks (TSQ) typically formed by a semipermeable pavement composed of light-colored cobblestones, gravel, or pebbles and with the presence of trees and small scattered garden areas with shrubbery.
- Parks and garden areas (PPG) mainly occupied by trees with hedge gardens and a combination of impervious and pervious pavements. This type includes pocket parks, walking paths, playgrounds, or sports fields.
- Pedestrian and transit areas (PIT) distributed throughout the city characterized by a combination of trees and predominantly impervious pavements like tails, asphalt, concrete, and in some cases, rubberized surfaces.
- Vegetated patches and public areas (HVP) for ornamental or structural purposes, with scattered trees and shrubs, mainly occupied by herbaceous vegetation and grass.
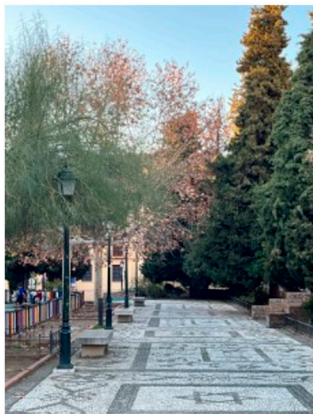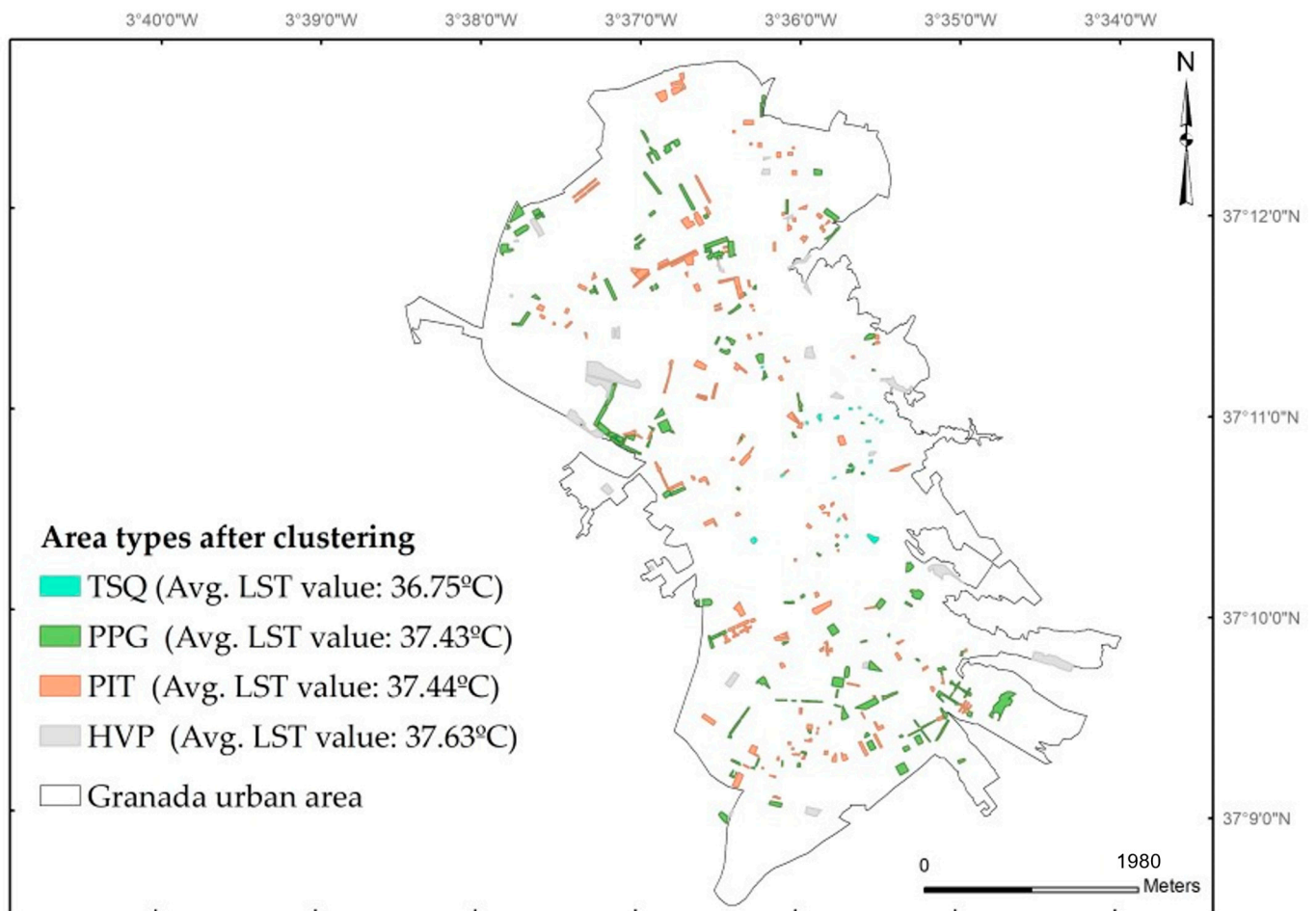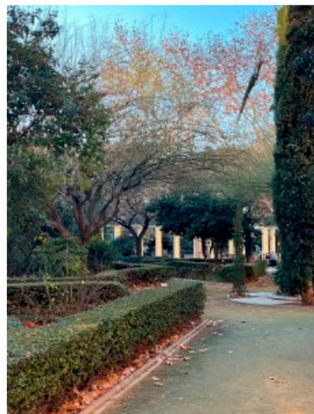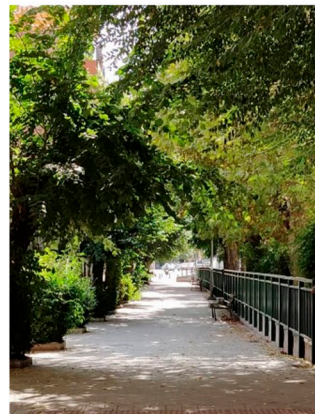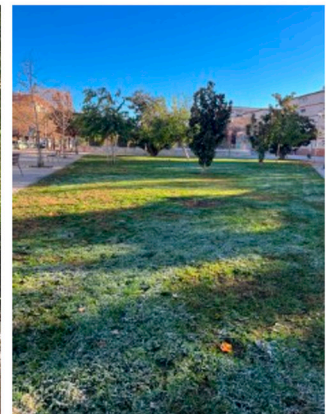
Figure 3. Area types resulting from clustering and examples. TSQ: Traditional squares; PPG: Parks and garden areas (PPG); PIT: Pedestrian and transit areas; HVP: Herbaceous vegetated patches.

Table 5. Percentage average of composition elements per defined area type.

Composition Element	Defined Area Type after Clustering			
	TSQ	PPG	PIT	HVP
Tree	14.52%	42.07%	18.95%	10.55%
Shrub	5.72%	9.19%	6.09%	8.08%
Herbaceous/Grass	0.27%	6.77%	2.17%	73.43%
Soil	0.17%	4.48%	0.47%	1.27%
Pervious surface	0.68%	18.95%	3.34%	2.05%
Impervious surface	5.64%	17.41%	67.92%	3.97%
Build	0.04%	0.14%	0.69%	0.67%
Water	0.04%	0.09%	0.11%	0.00%
Cobblestone/gravel/pebble	72.93%	0.98%	0.22%	0.00%

TSQ: Traditional squares; PPG: Pocket Parks and gardens; PIT: Pedestrian areas mainly covered by impervious surfaces and trees; HVP: herbaceous and grass vegetated patches.

Upon defining the area types through clustering, additional analysis included calculating the average LST value for each cluster across all episodes. The lowest average LST was observed in TSQ areas (36.75 °C), whereas PIT and PPG areas exhibited quite similar values (37.44 °C and 37.43 °C, respectively). Finally, HVP areas showed the highest average LST values across all episodes, with a value of 37.63 °C (Figure 3).

3.3. Regression Results

The ordinal regression analysis examining the relationship between ranges of maximum LST values and composition elements demonstrated statistically significant ($p < 0.05$) model fitting information across most episodes, except for episode 8. Estimates with a significance level of <0.05 showcased distinct relationships between these two variables accordingly (Table 6).

Composition elements such as trees, shrubs, impervious surfaces and cobblestone, and gravel and pebble surfaces were identified as significant factors in predicting the variability in LST ranges. For every one-unit increase in any of these variables, a decrease in the ordered log odds of reaching the highest LST range (maximum values above 41 °C) was expected. The presence of trees exhibited a negative directional relationship in episodes HW1 (estimate: −0.51), HW6 (estimate: −0.57), HW7 (estimate: −1.83), HW9 (estimate: −0.54), HW15 (estimate: −0.38), and HW16 (estimate: −0.40). There was a predicted decrease of −0.40 in the logarithmic probability of reaching the highest LST range considering all episodes. Similarly, the presence of shrubs demonstrated a negative directional relationship in episodes HW9 (estimate: −0.65), HW15 (estimate: −0.66), and HW16 (estimate: −0.67). The presence of impervious surfaces exhibited a negative direction in episodes HW7 (estimate: −1.23) and HW9 (estimate: −0.41). Furthermore, presence of cobblestone, gravel, and pebble surfaces showed a consistent negative direction in episodes HW1 to HW6 (estimates: −0.49, −0.43, −0.57), HW9 (estimate: −0.47), and HW15 (estimate: −0.41), as well as a predicted decrease in the logarithmic probability (estimate: −0.41) of reaching the highest LST range in consideration of all episodes (Table 6).

In contrast, herbaceous vegetation and grass presence showed a positive directional relationship in episode HW11, indicating that for every range increase in herbaceous vegetation and grass as the area surface, there is a predicted increase of 0.55 in the relative probability of the LST range considered exceeding 41 °C. Estimates for the rest of the independent variables (bare soil, pervious surface, and building) did not show statistical significance in any of the models (Table 6). Water was excluded as a composition element in the regression models due to its virtually negligible presence in the study areas. Water was only present in 16 out of the 341 areas under investigation, and in none of these cases did the surface coverage percentage exceed 3% or 100 m^2.

Table 6. Ordinal regression analysis: estimates for LST range prediction based on composition elements.

	Episode; MFI Sig.		HW1 **	HW5 **	HW6 **	HW7 ***	HW8	HW9 **	HW10 *	HW11 **	HW12 *	HW15 ***	HW16 ***	All Ep. **
Threshold	LST Range 1		−8.16	−2.60	−6.31	−35.13		−9.19	−5.85	−1.50	−4.36	−8.89	−9.58	−7.36
	LST Range 2		−5.54	0.66	−3.05	−33.88	−4.33	−6.54	−3.79	2.11	−2.26	−6.29	−7.47	−3.93
	LST Range 3		−2.15	3.34	−1.33	−33.17	−2.84	−3.62	−0.14	5.30	1.11	−2.94	−4.70	−0.51
	LST Range 4		−0.58	4.21	0.18		0.12	−2.20	2.45	6.76	4.16	−0.19	−1.99	1.54
Location	Tree	**Model Parameters (β)**	−0.51 *	0.00	−0.57 *	−1.83 *	−0.08	−0.54 *	−0.26	0.00	0.06	−0.38 *	−0.40 *	−0.40 *
	Shrub		−0.51	−0.37	−0.53	−1.77	−0.39	−0.65 *	−0.24	−0.26	−0.29	−0.66 *	−0.67 *	−0.59
	Herb/Grass		0.01	0.15	−0.08	−0.65	0.32	−0.06	0.27	0.55 *	0.36	0.22	0.24	0.16
	Soil		−0.55	0.07	−0.52	−9.29	0.38	−0.26	−0.16	0.15	0.00	−0.43	−0.17	−0.32
	Perv. Surf.		−0.04	0.37	−0.06	−0.70	0.17	−0.08	0.14	0.29	0.23	0.05	0.11	0.16
	Imp. Surf.		−0.35	0.00	−0.35	−1.23 *	−0.02	−0.41 *	−0.11	0.16	−0.02	−0.14	−0.23	−0.25
	Build		−0.35	0.41	−0.64	−11.52	0.04	−1.62	0.28	1.96	1.28	−0.47	−1.42	−0.05
	C/G/P		−0.49 *	−0.43 *	−0.57 *	−7.44	−0.24	−0.47 *	−0.21	−0.04	−0.22	−0.41 *	−0.29	−0.37

MFI: Model fitting information. * Sig. < 0.05; ** Sig. < 0.01; *** Sig. < 0.001.

Table 7. Ordinal regression analysis: estimates and model parameters for LST range prediction based on area type.

	Episode; MFI Sig.		HW1	HW5 **	HW6 *	HW7	HW8 *	HW9	HW10 *	HW11 **	HW12 **	HW15 **	HW16 **	All Ep. *
Threshold	LST Range 1		−4.92	−2.88	−2.20	2.16		−4.25	−6.18	−6.05	−6.63	−6.87	−7.02	−5.56
	LST Range 2		−2.29	0.38	0.92	3.38	−5.28	−1.61	−4.12	−2.43	−4.52	−4.26	−4.92	−2.14
	LST Range 3		0.94	2.97	2.62	4.07	−3.79	1.16	−0.50	0.74	−1.14	−0.96	−2.17	1.09
	LST Range 4		2.49	3.89	4.12		−0.84	2.57	2.05	2.17	1.87	1.65	0.41	3.12
Location	TSQ	**Model Parameters (β)**	−1.67	−1.79 **	−1.70 *	−20.13	−1.94 **	−1.44	−1.86 **	−2.16 ***	−1.99 **	−2.22 ***	−1.93 ***	−1.68 **
	PPG		−0.88	0.11	−0.60	−0.75	−0.79	−0.55	−0.99 *	−1.47 ***	−0.60	−1.06 *	−1.10 *	−0.74
	PIT		−0.91	0.04	−0.67	−1.79	−0.78	−0.67	−1.09 *	−1.18 **	−0.80 *	−0.88 *	−1.27 **	−0.88 *
	HVP		0 [a]	0 [a]	0 [a]	0 [a]	0 [a]	0 [a]	0 [a]	0 [a]	0 [a]	0 [a]	0 [a]	0 [a]

MFI: Model fitting information. * Sig. < 0.05; ** Sig. < 0.01; *** Sig. < 0.001. [a]: parameter is set to zero because it is redundant.

The models relating ranges of maximum LST values and type of area values exhibited model fitting statistical significance ($p < 0.05$) for every episode, except for episodes HW1, HW7, and HW9. In consideration of all episodes, statistical significance ($p < 0.05$) was also observed for the whole model. In this ordinal regression analysis, estimates for areas TSQ, PPG, and PIT showed statistically significant explanatory strength with the variability of LST ranges, compared to area type HVP (Table 7).

For TSQ areas, a negative directional relationship was observed, indicating a significant predicted decrease in the logarithmic probability of reaching the highest LST range in episodes HW5 (estimate: −1.79), HW6 (estimate: −1.70), HW10 (estimate: −1.86), HW11 (estimate: −2.16), HW12 (estimate: −1.99), HW15 (estimate: −2.22), and HW16 (estimate: −1.93). In episode HW8, a negative estimate (−1.94) showed a decrease in the relative probability of reaching the minimum LST range (up to 35 °C) and surpassing the highest one (over 41 °C). For PPG areas, results showed statistically significant negative estimates in episodes HW10 (−0.99), HW11 (−1.47), HW15 (−1.06), and HW16 (−1.10), indicating a decrease in the log odds of attaining Range 5 of maximum LST values compared to the reference area type. Results with statistical significance for PIT areas displayed negative estimates in episodes HW10 (−1.09), HW11 (−1.18), HW12 (−0.80), HW15 (−0.88), and HW16 (−1.27), indicating the association with the variability in the LST ranges explored in this analysis. In consideration of all episodes, a predicted decrease in the relative probability of reaching the highest LST range was observed for areas TSQ and PIT compared to HVP areas. The result for TSQ areas (estimate: −1.68) showed higher explanatory strength and stronger significance than that for PIT areas (estimate: −0.88) for decreasing the relative probability of exceeding the highest threshold set within the LST ranges (above 41 °C) (Table 7).

Finally, the regressions performed between orientation as the independent variable and LST ranges as the dependent variable did not show statistical significance for any of the episodes or for all episodes combined (model fitting information sig. > 0.05 in all cases). Therefore, the results have not been included in this article.

4. Discussion

This study carried out an investigation into the variability of land surface temperature (LST) values during different heat wave (HW) episodes from 2017 to 2023 in the city of Granada. The analysis focused on target areas within the urban green infrastructure (UGI), specifically on smaller public urban green spaces (SPUGS), characterized by varying percentages of different compositional elements. To address the existing challenges in the interpretation of LST values and the relationship with the capability of UGI assets to mitigate heat stress derived from higher surface temperatures [72], the study considered spatio-temporal scales and thermal comfort aspects.

The observed trend in the intensity and duration of HW in our study area aligns with the findings of existing research in the Mediterranean region [73]. Following the most intense HW episode (25 July to 2 August 2020), where 98.83% of areas recorded values above 39.01 °C, a slightly upward trend was observed thereafter. The last three episodes recorded in July 2022 and August 2023 registered LST values for all areas that fell into the upper ranges, surpassing the 39.01 °C threshold. (Figure 2, Table 3). In addition to the increased intensity, the affected area during HW tended to expand, consistent with similar findings in the Mediterranean region [74]. While most target areas recorded LST values below 39.01 °C in the initial episodes (2017–2019), more than 75% of the areas registered values above 37.01 °C from episodes in August 2020 onwards, reaching this proportion in over 96% of the last episodes during the years 2022 and 2023 (Table 3). Specifically, the average extent of HWs in the Iberian Peninsula is expected to range from 6% to 8% per decade in the near future [75]. This increasing trend in spatial extent of HWs under future climate conditions implies heightened human exposure among other associated effects such as ecological, natural risk, and energy impacts [76,77].

Regarding the statistical analysis of the relationship between reached LST ranges and composition elements, the ordinal regression models did not yield statistically significant results for episode HW8, the most intense one. Episode HW8, spanning from 25 July to 2 August 2020, presented the highest land surface temperature (LST) values during the study period. In comparison to the year 2023, the year 2020 had the highest average temperatures recorded in the months leading up August [78]. Exploring further the particularity of HW8, it is noteworthy to acknowledge that previous analyses conducted in the Mediterranean region underscored the significant role of variables predicting and influencing LST, especially solar radiation at the same geographical point and elevation [79]. Solar radiation, especially during the hours for which we retrieved data for this study, is affected not only by climate factors, such as temperature, relative humidity, wind direction, precipitation, wind speed, and cloud cover, but also by the presence of air pollutants [80]. In this context, considering the most intense heatwaves, HW8 (July 2020) and HW16 (August 2023), the air quality in July 2020, preceding HW8, was worse than that in August 2023, preceding HW16. Specifically, and for indicative purposes, 45.2% of days in July 2020 exhibited regular or poor air quality (based on the European Air Quality Index) [81], whereas the percentage of days with regular or poor air quality was 29% in August 2023 [82]. This observation might suggest that air quality and pollution levels preceding a heat wave may exacerbate LST values. Furthermore, the role of smaller green spaces in their interactions with air quality becomes even more relevant [83,84]. Additionally, it would be interesting to investigate if, under extreme heat conditions like those of this episode, thermal stress is so severe that only strategies like shading [85] or ventilation [86] prove to be the most effective in mitigating the impacts of warm spells.

However, the regression model based on the percentage of composition elements did provide significant information for the remaining episodes (Table 6). Vegetation composition elements, represented by the independent variables trees and shrubs, contributed significantly to explaining the avoidance of reaching the highest LST range. This highlights the effective role of trees and shrubs in mitigating extreme LST values [87]. The observed capability of trees to decrease the logarithmic probability of reaching the highest LST range (above 41.01 °C) is particularly effective in Mediterranean regions [88,89]; this is also the case for shrubs and other smaller-sized species [90], which showed a statistically significant capacity to decrease the log odds of reaching the highest LST range in our study, albeit in fewer episodes. This capacity reached its peak strength in the least intense episode (HW7), where trees and impervious surfaces showed significant results. This association of variables might, on occasion, generate this negative direction in the relative probability of reaching higher LST values [91].

The presence of cobblestone, gravel, and pebbles (C/G/P) pavements as a composition element showed significant coefficients with a negative direction in episodes HW1, HW5, HW6, HW9, and HW15. The significance and directional relationship observed for the variable "C/G/P" in the model considering all episodes suggest that the presence of this type of surface might favor a decrease in the relative probability of falling within the LST range of maximum values, corresponding to the hottest one (above 41 °C), and could help counteract warming and the impact of hot extremes [92,93]. Aggregates of light-colored C/G/P have intrinsic high albedo and emittance [94], which are key characteristics for maintaining lower surface temperatures when exposed to solar radiation and reducing surface and air temperatures [35,95]. In this study, this outcome aligns with findings obtained in the Mediterranean region, where highly reflective materials have demonstrated effectiveness in reducing surface temperature and mitigating the impacts of heat waves [96]. However, pavements of C/G/P may not be the most suitable in terms of usability, physical barrier management, and coverage guidelines of universal urban green area design [97,98].

The only composition element that presented a positive coefficient, and therefore a predicted increase in the log odds of reaching the highest LST range, was herbaceous species and grass in the HW11 episode (June 2022). According to the official regional environmental information network for the study area (Environmental Information Net-

work of Andalusia—REDIAM), within the years under consideration in the study, 2022 in Granada exhibited, on the on hand, the highest vegetation water stress index (ratio between stressed and non-stressed vegetation) and, on the other hand, one of the lowest monthly average precipitations for the month of June (1.3 L/m^2) [99]. Herbaceous vegetation and grass can reach very high temperatures in the absence of evapotranspiration, and their positive impact on air temperature and, consequently, pedestrian heat stress, strongly rely on irrigation, so when this type of land cover becomes dry, the surface temperature can increase, negating its positive impact [100,101].

Composition elements, such as soil and buildings, both with the lowest average coverage percentages (Table 4), were found to be not significant predictors of LST variation. Specifically, concerning the soil composition element, the outcomes differed from potentially expected results, as dry and heat-stressed soil typically contributes to a positive feedback of increased air and surface temperatures [102,103]. Regarding buildings, the types found in the target areas are mainly kiosks or small maintenance infrastructures, and the lack of significance could be related to, besides their limited presence, the specific types of buildings identified, as low-height structures might not contribute significantly to heat stress [104]. Similarly, pervious surfaces were also identified as not significant predictors of LST variation. In this case, the relatively low presence in the target areas might explain the lack of significance, as their effects become more noticeable when larger extensions are present [105] or in climates with milder temperatures than the Mediterranean region, featuring limited seasonal variations and more evenly distributed precipitation throughout the year [106].

The identified area types resulting from clustering exhibit similarities with other studies that classify green infrastructure typologies based on impervious, pervious, and mixed pavements combining different vegetation types (trees, grass, and shrubs) with irrigated and non-irrigated surfaces [107], studies where urban green areas categories are based on usage (commercial, residential, or mixed-use) [108], or studies using local climate zones characterized by building typology and the amount of vegetated surface as drivers for heat-stress-related research [109]. However, the area types obtained after clustering in this study are more specific to the study area, which enhances the granularity and accuracy of the study, aligning it more closely with the actual conditions and features of the local UGI.

The regression models exploring the relationship between LST values and the type of area defined after clustering demonstrated statistical significance (sig. model fitting information < 0.05) for all episodes (except HW1, HW7, and HW9) and for all episodes as a whole. Using areas defined as "Vegetated patches and public areas with scattered trees and shrubs, mainly occupied by herbaceous vegetation and grass" (HVP) as a reference, which exhibited higher average LST values (Figure 3), all other area types consistently performed better in terms of reducing the relative probability of reaching LST Range 5 (over 41 °C) (Table 7). Thus, this result could be interpreted as indicating a lower cooling effectiveness of the HVP areas. This may be attributed to their heavy reliance on substantial irrigation for herbaceous and grass covers, which is often challenging in climates like that of the study area, where soil water availability is frequently a limiting factor [110].

Consistent with previous research, among the technologies for reducing both air and surface temperatures and consequently improving outdoor thermal comfort, including cool pavements, greenery, solar control, shading, or spray systems, the combination of these technologies provides better outcomes than the use of technologies individually in terms of thermal comfort improvement [111]. In particular, urban greenery, especially trees, as well as the combination of trees and hedges, have a high potential for mitigating heat stress. However, non-vegetated surfaces, such as reflective pavements, also have a cooling effect, and combined with greening strategies, the capacity to reduce the effect of extreme temperatures can be enhanced [112].

Notably, traditional squares and parks, characterized by semipermeable pavements made of cobblestones, gravel, or pebbles, along with the presence of trees and small scattered garden areas with shrubbery (TSQ), exhibited statistically significant associations

with attained temperatures compared to HVP areas. The coefficients displayed by TSQ areas showed a consistently negative relationship in each HW episode (except HW1 and HW9) and when considering all episodes. This negative relationship suggests their potential capacity to decrease the relative probability of surpassing LST values of 41 °C. These areas feature surfaces composed of high-albedo reflective pavements with porous interstitial spaces, representing a structural coverage type that has a significant influence in reducing heat stress, at both surface and air levels, by increasing cooling effectiveness [113,114]. Furthermore, the stronger direction of the relationship observed for TSQ areas compared to areas with more vegetation, such as PPG areas, highlights how the cooling potential of urban trees may not be that high during warm spells, particularly in the Mediterranean region, where projected drying summers can potentially reduce vegetation benefits, making the influence of high-albedo materials, like C/G/P pavements, more relevant in this region [115]. In this context, it is noteworthy that, while the regression model does not yield significant parameters in the variation of LST for individual composition elements during HW8 (the most intense episode) (Table 6), it does so for traditional square (TSQ) areas in that specific warm spell (Table 7). The distinctive behavior of TSQ areas, compared to others during this particular episode, could be attributed to two main factors. On the one hand, the presence of reflective pavements on urban ground surfaces has been demonstrated to significantly reduce surface temperatures and convective heat release into the surrounding air so they have can offer widespread cooling benefits [116,117]. On the other hand, for effective heat stress reduction, a combination of greenery strategies and the use of cool building materials, such as urban paving with heat-resistant designs, can contribute to the cooling capacity of urban settings during heat wave episodes [118]. The synergistic integration of highly reflective materials with street trees, as observed in our study in TSQ areas, appears to be a highly effective approach for ambient air cooling and managing increased reflected solar radiation [119]. Additionally, combining street trees with cool pavements is demonstrated to be an efficient method for preserving pedestrians' outdoor thermal comfort, particularly in the Mediterranean climate [104].

Compared to HVP areas, parks and garden areas mainly occupied by trees with hedge gardens (PPG) and pedestrian and transit areas with presence of trees and impervious pavements (PIT) showed similar results and were more likely to indicate a decrease in the relative probability of exceeding LST ranges over 41 °C from episode HW10 onwards (with an exception in episode HW12 for PPG). Regarding PPG areas, results of this study are consistent with previous research proving the capacity of vegetation in the Mediterranean dense urban matrix to mitigate the impacts of HW episodes' heat stress conditions [17,120,121]. However, considering all episodes, only in PIT areas did the coefficients indicate a statistically significant negative direction in the log odds probability of surpassing 41 °C (LST range 5). Despite the capacity of PPG areas to ameliorate the impact of warm spells, mainly due to the presence of trees, they may not fully compensate for the effects of impervious surfaces in reducing LST. These effects can persist beyond the night hours (note that the retrieved Landsat images were acquired in the morning hours), and the determination of a location's LST and, consequently, its microclimate conditions, may not solely depend on the extent of tree cover but also on the presence of shade [110,122]. Additionally, the presence of plastic-based impervious surface coatings (rubber and cast rubber) in PPG areas excessively increases LST values, generating extreme surface temperatures [123]. Furthermore, the combination of pavements found in PIT areas, along with the inclusion of trees, can create highly effective conditions to alleviate the effects of episodes of extreme heat in certain urban geometries [124]. These considerations would indicate the importance of planning new UGI areas and rethinking the designs of existing ones, to enhance well-being conditions during extreme heat episodes [125]. Furthermore, the significance of strategically placing vegetation in heat-exposed areas seems to be more effective in mitigating the impacts of HW than merely aiming for an increase in the percentage of green coverage [126].

Finally, the regression models based on the orientation of the areas suggests that this variable is not a significant predictor in the variability of LST values during the recorded

HW episodes, despite orientation being a condition that can potentially influence the impacts of warm spells due to its influence on the duration of shading periods and urban ventilation [57]. The lack of significance in this study could be attributed to the fact that orientation tends to be more influential in linear geometries, such as street canyons or connectors between UGI patches [127,128]. It is indeed important to acknowledge certain limitations in this study. Firstly, ventilation and shade effects were not considered as independent variables in the regression models. The absence of these factors might introduce some level of incompleteness to the assessment, as both ventilation and shading can significantly influence local microclimates and subsequently impact LST values. Future studies could benefit from incorporating these variables to provide a more comprehensive understanding of the thermal dynamics in urban green spaces during HW episodes. Furthermore, there are additional variables that warrant further investigation for a more nuanced analysis. Among these, the typology and phenology of plant species emerge as crucial factors influencing their adaptability and resilience to present and future climatic conditions. A more detailed exploration of these aspects could contribute valuable insights into the effectiveness of different vegetation types in mitigating HW impacts throughout UGI areas in Mediterranean urban environments [129–131]. Additionally, it is worth noting that nighttime conditions provide complementary information for a more exhaustive evaluation of the urban green spaces' cooling effects across the entire diurnal cycle. In subsequent research, examining the impact of external factors beyond UGI management, such as meteorological conditions (e.g., atmospheric circulation and cloudiness) and air quality, and considering urban planning and architecture for both existing and newly developed areas, could offer valuable insights into the influence on LST.

5. Conclusions

In conclusion, from the heat wave (HW) episodes analyzed since 2017, this study revealed how LST ranges increased across numerous areas, highlighting heightened thermal stress in a Mediterranean medium-sized compact city. Trees played a crucial role in lowering the log odds of reaching higher LST range (above 41 °C). Cobblestone, gravel, and pebble (C/G/P) pavements also showed potential in decreasing this probability. Herbaceous species and grass cover, however, exhibit a positive coefficient in one of the episodes, indicating higher relative probability of reaching higher surface temperatures. Orientation and certain composition elements, like soil and buildings, did not significantly influence LST variation.

Among area types, traditional squares and parks (TSQ), pocket parks and gardens (PPG), and pedestrian areas with trees and impervious surfaces (PIT) performed better than vegetated patches (HVP) in reducing the probability of exceeding LST Range 5 (above 41 °C). The study advocates for strategically placing vegetation in heat-exposed areas, coupled with pavements like C/G/P, as an alternative strategy to simply increasing green coverage. Therefore, UGI areas´ design, combining trees with reflective pavements, proved its potential effectiveness in mitigating HW impacts.

Future research should explore granular aspects like pavement types, shading, ventilation, and plant resilience to refine our understanding of these relationships at smaller spatial scales.

In summary, this study not only advances our understanding of LST dynamics during HW episodes, but also guides strategies for enhancing the resilience of urban green spaces during extreme heat events.

Author Contributions: Conceptualization, M.J.D.-C.; methodology, M.J.D.-C., P.C. and P.E.-C.; software, M.J.D.-C. and P.E.-C.; validation, M.J.D.-C. and P.C.; formal analysis, M.J.D.-C. and P.C.; investigation, M.J.D.-C.; resources, M.J.D.-C.; data curation, M.J.D.-C. and P.E.-C.; writing—original draft preparation, M.J.D.-C.; writing—review and editing, M.J.D.-C., P.C. and P.E.-C.; visualization, M.J.D.-C.; supervision, M.J.D.-C. and P.C. All authors have read and agreed to the published version of the manuscript.

Data Availability Statement: Publicly available datasets were analyzed in this study. These data can be found here: https://www.usgs.gov/ (accessed on 10 October 2023); https://www.juntadeandalucia.es/ (accessed on 10 October 2023).

Conflicts of Interest: The authors declare no conflicts of interest.

References

1. Marx, W.; Haunschild, R.; Bornmann, L. Heat waves: A hot topic in climate change research. *Theor. Appl. Climatol.* **2021**, *146*, 781–800. [CrossRef]
2. Breshears, D.D.; Fontaine, J.B.; Ruthrof, K.X.; Field, J.P.; Feng, X.; Burger, J.R.; Law, D.J.; Kala, J.; Hardy, G.E.S.J. Underappreciated plant vulnerabilities to heat waves. *New Phytol.* **2021**, *231*, 32–39. [CrossRef]
3. Santamouris, M. Recent progress on urban overheating and heat island research. Integrated assessment of the energy, environmental, vulnerability and health impact. Synergies with the global climate change. *Energy Build.* **2020**, *207*, 109482. [CrossRef]
4. World Meteorological Organization. Available online: https://public.wmo.int/en (accessed on 20 February 2023).
5. Data.GISS: GISS Surface Temperature Analysis (GISTEMP v4). Available online: https://data.giss.nasa.gov/gistemp/ (accessed on 18 January 2024).
6. IPCC Working Groups I II. IPCC Synthesis Report of the Sixth Assessment Report. 2022. Available online: https://www.ipcc.ch/ar6-syr/ (accessed on 20 December 2022).
7. Perkins-Kirkpatrick, S.E.; Lewis, S.C. Increasing trends in regional heatwaves. *Nat. Commun.* **2020**, *11*, 3357. [CrossRef] [PubMed]
8. Hochman, A.; Mercogliano, P.; Alpert, P.; Saaroni, H.; Bucchignani, E. High-resolution projection of climate change and extremity over Israel using COSMO-CLM. *Int. J. Climatol.* **2018**, *38*, 5095–5106. [CrossRef]
9. Wedler, M.; Pinto, J.G.; Hochman, A. More frequent, persistent, and deadly heat waves in the 21st century over the Eastern Mediterranean. *Sci. Total Environ.* **2023**, *870*, 161883. [CrossRef] [PubMed]
10. Donateo, A.; Palusci, O.; Pappaccogli, G.; Esposito, A.; Martilli, A.; Santiago, J.L.; Buccolieri, R. Analysis of urban heat island and human thermal comfort in a Mediterranean city: A case study of Lecce (Italy). *Sustain. Cities Soc.* **2023**, *98*, 104849. [CrossRef]
11. Hochman, A.; Marra, F.; Messori, G.; Pinto, J.G.; Raveh-Rubin, S.; Yosef, Y.; Zittis, G. Extreme weather and societal impacts in the eastern Mediterranean. *Earth Syst. Dyn.* **2022**, *13*, 749–777. [CrossRef]
12. Lange, M.A. Climate Change in the Mediterranean: Environmental Impacts and Extreme Events. *IEMed Mediterr. Yearb.* **2020**, *2020*, 30–45.
13. Song, J.; Lu, Y.; Fischer, T.; Hu, K. Effects of the urban landscape on heatwave-mortality associations in Hong Kong: Comparison of different heatwave definitions. *Front. Environ. Sci. Eng.* **2024**, *18*, 11. [CrossRef]
14. Cuerdo-Vilches, T.; Díaz, J.; López-Bueno, J.A.; Luna, M.Y.; Navas, M.A.; Mirón, I.J.; Linares, C. Impact of urban heat islands on morbidity and mortality in heat waves: Observational time series analysis of Spain's five cities. *Sci. Total Environ.* **2023**, *890*, 164412. [CrossRef]
15. Royé, D.; Codesido, R.; Tobías, A.; Taracido, M. Heat wave intensity and daily mortality in four of the largest cities of Spain. *Environ. Res.* **2020**, *182*, 109027. [CrossRef]
16. López-Bueno, J.A.; Díaz, J.; Sánchez-Guevara, C.; Sánchez-Martínez, G.; Franco, M.; Gullón, P.; Núñez Peiró, M.; Valero, I.; Linares, C. The impact of heat waves on daily mortality in districts in Madrid: The effect of sociodemographic factors. *Environ. Res.* **2020**, *190*, 109993. [CrossRef]
17. Iungman, T.; Cirach, M.; Marando, F.; Pereira Barboza, E.; Khomenko, S.; Masselot, P.; Quijal-Zamorano, M.; Mueller, N.; Gasparrini, A.; Urquiza, J.; et al. Cooling cities through urban green infrastructure: A health impact assessment of European cities. *Lancet* **2023**, *401*, 577–589. [CrossRef] [PubMed]
18. Diz-Mellado, E.; López-Cabeza, V.P.; Rivera-Gómez, C.; Galán-Marín, C.; Rojas-Fernández, J.; Nikolopoulou, M. Extending the adaptive thermal comfort models for courtyards. *Build. Environ.* **2021**, *203*, 108094. [CrossRef]
19. Natanian, J.; Kastner, P.; Dogan, T.; Auer, T. From energy performative to livable Mediterranean cities: An annual outdoor thermal comfort and energy balance cross-climatic typological study. *Energy Build.* **2020**, *224*, 110283. [CrossRef]
20. Hidalgo-García, D.; Arco-Díaz, J. Modeling the Surface Urban Heat Island (SUHI) to study of its relationship with variations in the thermal field and with the indices of land use in the metropolitan area of Granada (Spain). *Sustain. Cities Soc.* **2022**, *87*, 104166. [CrossRef]

21. Kumar, P.; Debele, S.E.; Sahani, J.; Aragão, L.; Barisani, F.; Basu, B.; Bucchignani, E.; Charizopoulos, N.; Di Sabatino, S.; Domeneghetti, A.; et al. Towards an operationalisation of nature-based solutions for natural hazards. *Sci. Total Environ.* **2020**, *731*, 138855. [CrossRef] [PubMed]

22. Panagiotakis, E.; Kolokotsa, D.; Chrysoulakis, N. Evaluation of nature-based solutions implementation scenarios, using urban surface modelling. *Green Energy Sustain.* **2021**, *1*, 0003. [CrossRef]

23. Perini, K.; Calise, C.; Castellari, P.; Roccotiello, E. Microclimatic and Environmental Improvement in a Mediterranean City through the Regeneration of an Area with Nature-Based Solutions: A Case Study. *Sustainability* **2022**, *14*, 5847. [CrossRef]

24. Maggiotto, G.; Miani, A.; Rizzo, E.; Castellone, M.D.; Piscitelli, P. Heat waves and adaptation strategies in a mediterranean urban context. *Environ. Res.* **2021**, *197*, 111066. [CrossRef] [PubMed]

25. Santamouris, M.; Osmond, P. Increasing Green Infrastructure in Cities: Impact on Ambient Temperature, Air Quality and Heat-Related Mortality and Morbidity. *Buildings* **2020**, *10*, 233. [CrossRef]

26. Delgado-Capel, M.J.; Cariñanos, P.; Escudero-Viñolo, M. Capacity of Urban Green Infrastructure Spaces to Ameliorate Heat Wave Impacts in Mediterranean Compact Cities: Case Study of Granada (South-Eastern Spain). *Land* **2023**, *12*, 1076. [CrossRef]

27. Coutts, A.M.; Harris, R.J.; Phan, T.; Livesley, S.J.; Williams, N.S.G.; Tapper, N.J. Thermal infrared remote sensing of urban heat: Hotspots, vegetation, and an assessment of techniques for use in urban planning. *Remote Sens. Environ.* **2016**, *186*, 637–651. [CrossRef]

28. Do Nascimento, A.C.L.; Galvani, E.; Gobo, J.P.A.; Wollmann, C.A. Comparison between Air Temperature and Land Surface Temperature for the City of São Paulo, Brazil. *Atmosphere* **2022**, *13*, 491. [CrossRef]

29. Benali, A.; Carvalho, A.C.; Nunes, J.P.; Carvalhais, N.; Santos, A. Estimating air surface temperature in Portugal using MODIS LST data. *Remote Sens. Environ.* **2012**, *124*, 108–121. [CrossRef]

30. Zhang, P.; Bounoua, L.; Imhoff, M.L.; Wolfe, R.E.; Thome, K. Comparison of MODIS Land Surface Temperature and Air Temperature over the Continental USA Meteorological Stations. *Can. J. Remote Sens.* **2014**, *40*, 110–122. [CrossRef]

31. Guo, A.; Yang, J.; Sun, W.; Xiao, X.; Xia Cecilia, J.; Jin, C.; Li, X. Impact of urban morphology and landscape characteristics on spatiotemporal heterogeneity of land surface temperature. *Sustain. Cities Soc.* **2020**, *63*, 102443. [CrossRef]

32. Aram, F.; Higueras García, E.; Solgi, E.; Mansournia, S.; García, E.H. Urban green space cooling effect in cities. *Heliyon* **2019**, *5*, e01339. [CrossRef]

33. Gallay, I.; Olah, B.; Murtinová, V.; Gallayová, Z. Quantification of the Cooling Effect and Cooling Distance of Urban Green Spaces Based on Their Vegetation Structure and Size as a Basis for Management Tools for Mitigating Urban Climate. *Sustainability* **2023**, *15*, 3705. [CrossRef]

34. Peng, J.; Dan, Y.; Qiao, R.; Liu, Y.; Dong, J.; Wu, J. How to quantify the cooling effect of urban parks? Linking maximum and accumulation perspectives. *Remote Sens. Environ.* **2021**, *252*, 112135. [CrossRef]

35. Wu, C.; Li, J.; Wang, C.; Song, C.; Haase, D.; Breuste, J.; Finka, M. Estimating the Cooling Effect of Pocket Green Space in High Density Urban Areas in Shanghai, China. *Front. Environ. Sci.* **2021**, *9*, 657969. [CrossRef]

36. Park, J.; Kim, J.H.; Lee, D.K.; Park, C.Y.; Jeong, S.G. The influence of small green space type and structure at the street level on urban heat island mitigation. *Urban For. Urban Green.* **2017**, *21*, 203–212. [CrossRef]

37. Hayes, A.T.; Jandaghian, Z.; Lacasse, M.A.; Gaur, A.; Lu, H.; Laouadi, A.; Ge, H.; Wang, L. Nature-Based Solutions (NBSs) to Mitigate Urban Heat Island (UHI) Effects in Canadian Cities. *Buildings* **2022**, *12*, 925. [CrossRef]

38. Jayasooriya, V.M.; Ng, A.W.M.; Muthukumaran, S.; Perera, C.B.J. Optimization of Green Infrastructure Practices in Industrial Areas for Runoff Management: A Review on Issues, Challenges and Opportunities. *Water* **2020**, *12*, 1024. [CrossRef]

39. Semeraro, T.; Scarano, A.; Buccolieri, R.; Santino, A.; Aarrevaara, E. Planning of Urban Green Spaces: An Ecological Perspective on Human Benefits. *Land* **2021**, *10*, 105. [CrossRef]

40. Cariñanos, P.; Ruiz-Peñuela, S.; Valle, A.M.; de la Guardia, C.D. Assessing pollination disservices of urban street-trees: The case of London-plane tree (*Platanus* x *hispanica* Mill. ex Münchh). *Sci. Total Environ.* **2020**, *737*, 139722. [CrossRef]

41. Kronenberg, J.; Haase, A.; Łaszkiewicz, E.; Antal, A.; Baravikova, A.; Biernacka, M.; Dushkova, D.; Filčak, R.; Haase, D.; Ignatieva, M.; et al. Environmental justice in the context of urban green space availability, accessibility, and attractiveness in postsocialist cities. *Cities* **2020**, *106*, 102862. [CrossRef]

42. Reyes-Riveros, R.; Altamirano, A.; De La Barrera, F.; Rozas-Vásquez, D.; Vieli, L.; Meli, P. Linking public urban green spaces and human well-being: A systematic review. *Urban For. Urban Green.* **2021**, *61*, 127105. [CrossRef]

43. Hidalgo García, D. Evaluation and Analysis of the Effectiveness of the Main Mitigation Measures against Surface Urban Heat Islands in Different Local Climate Zones through Remote Sensing. *Sustainability* **2023**, *15*, 10410. [CrossRef]

44. Clima de Andalucia. Available online: https://www.mapaclima.es/?variable=temperature_avg&year=2015-2040 (accessed on 15 December 2023).

45. Andrade, C.; Contente, J. Köppen's climate classification projections for the Iberian Peninsula. *Clim. Res.* **2020**, *81*, 71–89. [CrossRef]

46. World Maps of Köppen-Geiger Climate Classification. Available online: https://koeppen-geiger.vu-wien.ac.at/ (accessed on 19 February 2024).

47. AEMet. Listado de Provincias Afectadas por las Olas de Calor Registradas Desde 1975. 2023. Available online: https://www.aemet.es/documentos/es/conocermas/recursos_en_linea/publicaciones_y_estudios/estudios/Olas_calor/RelacionProvincias2021.pdf (accessed on 2 November 2023).

48. Delgado-Capel, M.; Cariñanos, P. Towards a Standard Framework to Identify Green Infrastructure Key Elements in Dense Mediterranean Cities. *Forests* **2020**, *11*, 1246. [CrossRef]

49. Peschardt, K.K.; Schipperijn, J.; Stigsdotter, U.K. Use of Small Public Urban Green Spaces (SPUGS). *Urban For. Urban Green.* **2012**, *11*, 235–244. [CrossRef]

50. Olas de Calor en España Desde 1975 Área de Climatología y Aplicaciones Operativas. Available online: https://www.aemet.es/documentos/es/conocermas/recursos_en_linea/publicaciones_y_estudios/estudios/Olas_calor/Olas_Calor_ActualizacionOctubre2021.pdf (accessed on 18 December 2023).

51. Landsat Normalized Difference Vegetation Index | U.S. Geological Survey. Available online: https://www.usgs.gov/landsat-missions/landsat-normalized-difference-vegetation-index (accessed on 1 December 2022).

52. Shi, Z.; Jia, G.; Zhou, Y.; Xu, X.; Jiang, Y. Amplified intensity and duration of heatwaves by concurrent droughts in China. *Atmos. Res.* **2021**, *261*, 105743. [CrossRef]

53. Mazdiyasni, O.; Sadegh, M.; Chiang, F.; Aghakouchak, A. Heat wave intensity Duration frequency curve: A Multivariate Approach for Hazard and Attribution Analysis. *Sci. Rep.* **2019**, *9*, 14117. [CrossRef]

54. Gobierno de España. Olas de Calor en España Desde 1975—Agencia Estatal de Meteorología—AEMET. Available online: https://www.aemet.es/documentos/es/conocermas/recursos_en_linea/publicaciones_y_estudios/estudios/Olas_calor/listadoprovinciasolascalor_1975_2023.pdf (accessed on 1 November 2023).

55. Goldblatt, R.; Addas, A.; Crull, D.; Maghrabi, A.; Levin, G.G.; Rubinyi, S. Remotely Sensed Derived Land Surface Temperature (LST) as a Proxy for Air Temperature and Thermal Comfort at a Small Geographical Scale. *Land* **2021**, *10*, 410. [CrossRef]

56. Kalogeropoulos, G.; Dimoudi, A.; Toumboulidis, P.; Zoras, S. Urban Heat Island and Thermal Comfort Assessment in a Medium-Sized Mediterranean City. *Atmosphere* **2022**, *13*, 1102. [CrossRef]

57. Lai, D.; Liu, W.; Gan, T.; Liu, K.; Chen, Q. A review of mitigating strategies to improve the thermal environment and thermal comfort in urban outdoor spaces. *Sci. Total Environ.* **2019**, *661*, 337–353. [CrossRef] [PubMed]

58. Gómez, F.; Cueva, A.P.; Valcuende, M.; Matzarakis, A. Research on ecological design to enhance comfort in open spaces of a city (Valencia, Spain). Utility of the physiological equivalent temperature (PET). *Ecol. Eng.* **2013**, *57*, 27–39. [CrossRef]

59. Höppe, P. The physiological equivalent temperature—A universal index for the biometeorological assessment of the thermal environment. *Int. J. Biometeorol.* **1999**, *43*, 71–75. [CrossRef] [PubMed]

60. Salata, F.; Golasi, I.; de Lieto Vollaro, R.; de Lieto Vollaro, A. Outdoor thermal comfort in the Mediterranean area. A transversal study in Rome, Italy. *Build. Environ.* **2016**, *96*, 46–61. [CrossRef]

61. Rodríguez-Algeciras, J.; Rodríguez-Algeciras, A.; Chaos-Yeras, M.; Matzarakis, A. Tourism-related climate information for adjusted and responsible planning in the tourism industry in Barcelona, Spain. *Theor. Appl. Climatol.* **2020**, *142*, 1003–1014. [CrossRef]

62. Cheung, P.K.; Jim, C.Y. Determination and application of outdoor thermal benchmarks. *Build. Environ.* **2017**, *123*, 333–350. [CrossRef]

63. Potchter, O.; Cohen, P.; Lin, T.P.; Matzarakis, A. Outdoor human thermal perception in various climates: A comprehensive review of approaches, methods and quantification. *Sci. Total Environ.* **2018**, *631–632*, 390–406. [CrossRef] [PubMed]

64. Kullmann, K. Landshape Urbanism. In *Companion to Public Space*; Routledge: London, UK, 2020.

65. Plan Nacional de Ortofotografía Aérea. Available online: https://pnoa.ign.es/ (accessed on 23 September 2023).

66. MohanRajan, S.N.; Loganathan, A.; Manoharan, P. Survey on Land Use/Land Cover (LU/LC) change analysis in remote sensing and GIS environment: Techniques and Challenges. *Environ. Sci. Pollut. Res.* **2020**, *27*, 29900–29926. [CrossRef]

67. Hiscock, O.H.; Back, Y.; Kleidorfer, M.; Urich, C. A GIS-based Land Cover Classification Approach Suitable for Fine-scale Urban Water Management. *Water Resour. Manag.* **2021**, *35*, 1339–1352. [CrossRef]

68. Zhou, Z.-H. Special Topic: Machine Learning A brief introduction to weakly supervised learning. *Natl. Sci. Rev.* **2018**, *5*, 44–53. [CrossRef]

69. Schmitt, M.; Prexl, J.; Ebel, P.; Liebel, L.; Zhu, X.X. Weakly Supervised Semantic Segmentation of Satellite Images for Land Cover Mapping-Challenges and Opportunities. *ISPRS Ann. Photogramm. Remote Sens. Spatial Inf. Sci.* **2020**, *3*, 795–802. [CrossRef]

70. Maalouf, M. Logistic regression in data analysis: An overview. *Int. J. Data Anal. Tech. Strat.* **2011**, *3*, 281–299. [CrossRef]

71. Cucchiara, A. Applied Logistic Regression. *Technometrics* **2012**, *34*, 358–359. [CrossRef]

72. Saaroni, H.; Amorim, J.H.; Hiemstra, J.A.; Pearlmutter, D. Urban Green Infrastructure as a tool for urban heat mitigation: Survey of research methodologies and findings across different climatic regions. *Urban Clim.* **2018**, *24*, 94–110. [CrossRef]

73. Molina, M.O.; Sánchez, E.; Gutiérrez, C. Future heat waves over the Mediterranean from an Euro-CORDEX regional climate model ensemble. *Sci. Rep.* **2020**, *10*, 8801. [CrossRef]

74. Pereira, S.C.; Marta-Almeida, M.; Carvalho, A.C.; Rocha, A. Heat wave and cold spell changes in Iberia for a future climate scenario. *Int. J. Climatol.* **2017**, *37*, 5192–5205. [CrossRef]

75. Lorenzo, N.; Díaz-Poso, A.; Royé, D. Heatwave intensity on the Iberian Peninsula: Future climate projections. *Atmos. Res.* **2021**, *258*, 105655. [CrossRef]

76. Schoetter, R.; Cattiaux, J.; Douville, H. Changes of western European heat wave characteristics projected by the CMIP5 ensemble. *Clim. Dyn.* **2015**, *45*, 1601–1616. [CrossRef]

77. Palipane, E.; Grotjahn, R. Future Projections of the Large-Scale Meteorology Associated with California Heat Waves in CMIP5 Models. *J. Geophys. Res. Atmos.* **2018**, *123*, 8500–8517. [CrossRef]

78. Gobierno de España. de Agencia Estatal de Meteorología—(AEMET). Available online: https://www.aemet.es/es/datos_abiertos/estadisticas (accessed on 15 February 2024).
79. Zhao, W.; Duan, S.B. Reconstruction of daytime land surface temperatures under cloud-covered conditions using integrated MODIS/Terra land products and MSG geostationary satellite data. *Remote Sens. Environ.* **2020**, *247*, 111931. [CrossRef]
80. Nisha Nandhini, R.; Geethakarthi, A. Influential Study and Development of Global Solar Radiation Prediction Model Using ANN. In Proceedings of the 2021 International Conference on Advancements in Electrical, Electronics, Communication, Computing and Automation (ICAECA), Coimbatore, India, 8–9 October 2021. [CrossRef]
81. European Air Quality Index. Available online: https://airindex.eea.europa.eu/Map/AQI/Viewer/ (accessed on 16 February 2024).
82. Ayto.Granada: Calidad del Aire. Available online: https://www.granada.org/inet/calidadaire.nsf (accessed on 15 February 2024).
83. Matos, P.; Vieira, J.; Rocha, B.; Branquinho, C.; Pinho, P. Modeling the provision of air-quality regulation ecosystem service provided by urban green spaces using lichens as ecological indicators. *Sci. Total Environ.* **2019**, *665*, 521–530. [CrossRef] [PubMed]
84. Hewitt, C.N.; Ashworth, K.; MacKenzie, A.R. Using green infrastructure to improve urban air quality (GI4AQ). *Ambio* **2020**, *49*, 62–73. [CrossRef]
85. Lin, T.P.; Matzarakis, A.; Hwang, R.L. Shading effect on long-term outdoor thermal comfort. *Build. Environ.* **2010**, *45*, 213–221. [CrossRef]
86. Ng, E. Policies and technical guidelines for urban planning of high-density cities—Air ventilation assessment (AVA) of Hong Kong. *Build. Environ.* **2009**, *44*, 1478–1488. [CrossRef] [PubMed]
87. Lai, S.; Leone, F.; Zoppi, C. Spatial Distribution of Surface Temperature and Land Cover: A Study Concerning Sardinia, Italy. *Sustainability* **2020**, *12*, 3186. [CrossRef]
88. Cohen, P.; Potchter, O.; Matzarakis, A. Daily and seasonal climatic conditions of green urban open spaces in the Mediterranean climate and their impact on human comfort. *Build. Environ.* **2012**, *51*, 285–295. [CrossRef]
89. Chatzidimitriou, A.; Yannas, S. Microclimate development in open urban spaces: The influence of form and materials. *Energy Build.* **2015**, *108*, 156–174. [CrossRef]
90. Marando, F.; Heris, M.P.; Zulian, G.; Udías, A.; Mentaschi, L.; Chrysoulakis, N.; Parastatidis, D.; Maes, J. Urban heat island mitigation by green infrastructure in European Functional Urban Areas. *Sustain. Cities Soc.* **2022**, *77*, 103564. [CrossRef]
91. Karimi, A.; Sanaieian, H.; Farhadi, H.; Norouzian-Maleki, S. Evaluation of the thermal indices and thermal comfort improvement by different vegetation species and materials in a medium-sized urban park. *Energy Rep.* **2020**, *6*, 1670–1684. [CrossRef]
92. Seneviratne, S.I.; Phipps, S.J.; Pitman, A.J.; Hirsch, A.L.; Davin, E.L.; Donat, M.G.; Hirschi, M.; Lenton, A.; Wilhelm, M.; Kravitz, B. Land radiative management as contributor to regional-scale climate adaptation and mitigation. *Nat. Geosci.* **2018**, *11*, 88–96. [CrossRef]
93. Kappou, S.; Souliotis, M.; Papaefthimiou, S.; Panaras, G.; Paravantis, J.A.; Michalena, E.; Hills, J.M.; Vouros, A.P.; Dimenou, K.; Mihalakakou, G. Cool Pavements: State of the Art and New Technologies. *Sustainability* **2022**, *14*, 5159. [CrossRef]
94. Oke, T.R. *Boundary Layer Climates*; Routledge: London, UK, 2002; ISBN 1134951337.
95. Noro, M.; Lazzarin, R. Urban heat island in Padua, Italy: Simulation analysis and mitigation strategies. *Urban Clim.* **2015**, *14*, 187–196. [CrossRef]
96. Falasca, S.; Ciancio, V.; Salata, F.; Golasi, I.; Rosso, F.; Curci, G. High albedo materials to counteract heat waves in cities: An assessment of meteorology, buildings energy needs and pedestrian thermal comfort. *Build. Environ.* **2019**, *163*, 106242. [CrossRef]
97. Piskin, B.A.; Akdeniz, N.S. How Can People with Disabilities Use the Outdoors? An Assessment Within the Framework of Disability Standards. *Soc. Indic. Res.* **2023**, *167*, 153–174. [CrossRef]
98. Wojnowska-Heciak, M.; Suchocka, M.; Błaszczyk, M.; Muszyńska, M. Urban Parks as Perceived by City Residents with Mobility Difficulties: A Qualitative Study with In-Depth Interviews. *Int. J. Environ. Res. Public Health* **2022**, *19*, 2018. [CrossRef] [PubMed]
99. Red de Información Ambiental de Andalucía—Portal Ambiental de Andalucía. Available online: https://www.juntadeandalucia.es/medioambiente/portal/acceso-rediam (accessed on 19 January 2024).
100. Parison, S.; Hendel, M.; Grados, A.; Royon, L. Analysis of the heat budget of standard, cool and watered pavements under lab heat-wave conditions. *Energy Build.* **2020**, *228*, 110455. [CrossRef]
101. Yang, J.; Wang, Z.H. Optimizing urban irrigation schemes for the trade-off between energy and water consumption. *Energy Build.* **2015**, *107*, 335–344. [CrossRef]
102. Benson, D.O.; Dirmeyer, P.A. Characterizing the Relationship between Temperature and Soil Moisture Extremes and Their Role in the Exacerbation of Heat Waves over the Contiguous United States. *J. Clim.* **2021**, *34*, 2175–2187. [CrossRef]
103. Stéfanon, M.; Drobinski, P.; D'Andrea, F.; Lebeaupin-Brossier, C.; Bastin, S. Soil moisture-temperature feedbacks at meso-scale during summer heat waves over Western Europe. *Clim. Dyn.* **2014**, *42*, 1309–1324. [CrossRef]
104. Salata, F.; Golasi, I.; Petitti, D.; de Lieto Vollaro, E.; Coppi, M.; de Lieto Vollaro, A. Relating microclimate, human thermal comfort and health during heat waves: An analysis of heat island mitigation strategies through a case study in an urban outdoor environment. *Sustain. Cities Soc.* **2017**, *30*, 79–96. [CrossRef]
105. Mohammad Harmay, N.S.; Choi, M. Effects of heat waves on urban warming across different urban morphologies and climate zones. *Build. Environ.* **2022**, *209*, 108677. [CrossRef]
106. Hendel, M.; Parison, S.; Grados, A.; Royon, L. Which pavement structures are best suited to limiting the UHI effect? A laboratory-scale study of Parisian pavement structures. *Build. Environ.* **2018**, *144*, 216–229. [CrossRef]

107. Bartesaghi-Koc, C.; Osmond, P.; Peters, A. Mapping and classifying green infrastructure typologies for climate-related studies based on remote sensing data. *Urban For. Urban Green.* **2019**, *37*, 154–167. [CrossRef]

108. Sabrin, S.; Karimi, M.; Nazari, R.; Pratt, J.; Bryk, J. Effects of Different Urban-Vegetation Morphology on the Canopy-level Thermal Comfort and the Cooling Benefits of Shade Trees: Case-study in Philadelphia. *Sustain. Cities Soc.* **2021**, *66*, 102684. [CrossRef]

109. Geletič, J.; Lehnert, M.; Dobrovolný, P.; Bechtel, B.; Keramitsoglou, I.; Kotthaus, S.; Voogt, J.A.; Zakšek, K.; Müller, R.; Thenkabail, P.S. Land Surface Temperature Differences within Local Climate Zones, Based on Two Central European Cities. *Remote Sens.* **2016**, *8*, 788. [CrossRef]

110. Elbondira, T.A.; Tokimatsu, K.; Asawa, T.; Ibrahim, M.G. Impact of neighborhood spatial characteristics on the microclimate in a hot arid climate—A field based study. *Sustain. Cities Soc.* **2021**, *75*, 103273. [CrossRef]

111. Bartesaghi-Koc, C.; Haddad, S.; Pignatta, G.; Paolini, R.; Prasad, D.; Santamouris, M. Can urban heat be mitigated in a single urban street? Monitoring, strategies, and performance results from a real scale redevelopment project. *Sol. Energy* **2021**, *216*, 564–588. [CrossRef]

112. Yenneti, K.; Ding, L.; Prasad, D.; Ulpiani, G.; Paolini, R.; Haddad, S.; Santamouris, M. Urban Overheating and Cooling Potential in Australia: An Evidence-Based Review. *Climate* **2020**, *8*, 126. [CrossRef]

113. Moretti, L.; Cantisani, G.; Carpiceci, M.; D'andrea, A.; Del Serrone, G.; Di Mascio, P.; Loprencipe, G. Effect of Sampietrini Pavers on Urban Heat Islands. *Int. J. Environ. Res. Public Health* **2021**, *18*, 13108. [CrossRef]

114. Santamouris, M. Using cool pavements as a mitigation strategy to fight urban heat island—A review of the actual developments. *Renew. Sustain. Energy Rev.* **2013**, *26*, 224–240. [CrossRef]

115. Schwaab, J.; Meier, R.; Mussetti, G.; Seneviratne, S.; Bürgi, C.; Davin, E.L. The role of urban trees in reducing land surface temperatures in European cities. *Nat. Commun.* **2021**, *12*, 6763. [CrossRef] [PubMed]

116. Schneider, F.A.; Ortiz, J.C.; Vanos, J.K.; Sailor, D.J.; Middel, A. Evidence-based guidance on reflective pavement for urban heat mitigation in Arizona. *Nat. Commun.* **2023**, *14*, 1467. [CrossRef] [PubMed]

117. Tsoka, S.; Tsikaloudaki, K.; Theodosiou, T.; Bikas, D. Urban Warming and Cities' Microclimates: Investigation Methods and Mitigation Strategies—A Review. *Energies* **2020**, *13*, 1414. [CrossRef]

118. Hatvani-Kovacs, G.; Bush, J.; Sharifi, E.; Boland, J. Policy recommendations to increase urban heat stress resilience. *Urban Clim.* **2018**, *25*, 51–63. [CrossRef]

119. Tsoka, S.; Tsikaloudaki, A.; Theodosiou, T. Analyzing the ENVI-met microclimate model's performance and assessing cool materials and urban vegetation applications—A review. *Sustain. Cities Soc.* **2018**, *43*, 55–76. [CrossRef]

120. Salata, F.; Golasi, I.; Vollaro, A.D.L.; Vollaro, R.D.L. How high albedo and traditional buildings' materials and vegetation affect the quality of urban microclimate. A case study. *Energy Build.* **2015**, *99*, 32–49. [CrossRef]

121. Rosso, F.; Cappa, F.; Spitzmiller, R.; Ferrero, M. Pocket parks towards more sustainable cities. Architectural, environmental, managerial and legal considerations towards an integrated framework: A case study in the Mediterranean region. *Environ. Chall.* **2022**, *7*, 100402. [CrossRef]

122. Bartesaghi-Koc, C.; Osmond, P.; Peters, A. Innovative use of spatial regression models to predict the effects of green infrastructure on land surface temperatures. *Energy Build.* **2022**, *254*, 111564. [CrossRef]

123. Bozdogan Sert, E.; Kaya, E.; Adiguzel, F.; Cetin, M.; Gungor, S.; Zeren Cetin, I.; Dinc, Y. Effect of the surface temperature of surface materials on thermal comfort: A case study of Iskenderun (Hatay, Turkey). *Theor. Appl. Climatol.* **2021**, *144*, 103–113. [CrossRef]

124. Mohammad, P.; Aghlmand, S.; Fadaei, A.; Gachkar, S.; Gachkar, D.; Karimi, A. Evaluating the role of the albedo of material and vegetation scenarios along the urban street canyon for improving pedestrian thermal comfort outdoors. *Urban Clim.* **2021**, *40*, 100993. [CrossRef]

125. Rey Gozalo, G.; Barrigón Morillas, J.M.; Montes González, D. Perceptions and use of urban green spaces on the basis of size. *Urban For. Urban Green.* **2019**, *46*, 126470. [CrossRef]

126. Zölch, T.; Maderspacher, J.; Wamsler, C.; Pauleit, S. Using green infrastructure for urban climate-proofing: An evaluation of heat mitigation measures at the micro-scale. *Urban For. Urban Green.* **2016**, *20*, 305–316. [CrossRef]

127. Lam, C.K.C.; Lee, H.; Yang, S.R.; Park, S. A review on the significance and perspective of the numerical simulations of outdoor thermal environment. *Sustain. Cities Soc.* **2021**, *71*, 102971. [CrossRef]

128. Karimi, A.; Mohammad, P.; García-Martínez, A.; Moreno-Rangel, D.; Gachkar, D.; Gachkar, S. New developments and future challenges in reducing and controlling heat island effect in urban areas. *Environ. Dev. Sustain.* **2022**, *25*, 10485–10531. [CrossRef]

129. Caneva, G.; Bartoli, F.; Zappitelli, I.; Savo, V. Street trees in italian cities: Story, biodiversity and integration within the urban environment. *Rend. Lincei* **2020**, *31*, 411–417. [CrossRef]

130. Morakinyo, T.E.; Ouyang, W.; Lau, K.K.L.; Ren, C.; Ng, E. Right tree, right place (urban canyon): Tree species selection approach for optimum urban heat mitigation—Development and evaluation. *Sci. Total Environ.* **2020**, *719*, 137461. [CrossRef] [PubMed]

131. Langenheim, N.; White, M.; Tapper, N.; Livesley, S.J.; Ramirez-Lovering, D. Right tree, right place, right time: A visual-functional design approach to select and place trees for optimal shade benefit to commuting pedestrians. *Sustain. Cities Soc.* **2020**, *52*, 101816. [CrossRef]